Acta Crystallographica Section C
Structural Chemistry
ISSN 2053-2296

Superconductivity of lithium-doped hydrogen under high pressure

Yu Xie,[a,b]‡ Quan Li,[a] Artem R. Oganov[b,c] and Hui Wang[a]*

[a]State Key Laboratory of Superhard Materials, Jilin University, Changchun 130012, People's Republic of China, [b]Department of Geosciences, Department of Physics and Astronomy, and New York Center for Computational Science, Stony Brook University, Stony Brook, NY 11794-2100, USA, and [c]Geology Department, Moscow State University, 119992 Moscow, Russian Federation
Correspondence e-mail: xiey@ornl.gov

Received 1 August 2013
Accepted 28 October 2013

The high-pressure lattice dynamics and superconductivity of newly proposed lithium hydrides (LiH_2, LiH_6 and LiH_8) have been extensively studied using density functional theory. The application of the Allen–Dynes modified McMillan equation and electron–phonon coupling calculations show that LiH_6 and LiH_8 are superconductors with critical temperatures (T_c) of 38 K at 150 GPa for LiH_6 and 31 K at 100 GPa for LiH_8, while LiH_2 is not a superconductor. The T_c of LiH_6 increases rapidly with pressure and reaches 82 K at 300 GPa due to enhancement of the electron–phonon coupling and the increased density of states at the Fermi level, while the T_c of LiH_8 remains almost constant.

Keywords: computational materials discovery; high-temperature superconductors; lithium hydrides; lithium-doped hydrogen; high-pressure studies.

1. Introduction

The search for high-temperature superconductor materials is one of the major thrusts in condensed matter physics. Hydrogen, the lightest element, exhibits many mysterious and nontrivial properties that remain elusive. The most fascinating and intriguing aspect of hydrogen is the possibility of high-temperature superconductivity (Ashcroft, 1968) in its metallic form (Barbee *et al.*, 1989; Wigner & Huntington, 1935) due to high vibrational frequencies and strong electron–phonon coupling under sufficiently strong compression. Despite many experimental efforts, the metallization of solid hydrogen has still not been observed, even at pressures of up to 342 GPa (Goncharov *et al.*, 2001; Loubeyre *et al.*, 2002). It has been suggested that hydrogen-dominated compounds, where the other components can be viewed as impurities, will metallize at much lower and more accessible pressures than those required for pure solid hydrogen, and may be potential high-temperature superconductors (Ashcroft, 2004). In these systems, hydrogen is perturbed by chemical bonding, *i.e.* 'chemically precompressed' (Ashcroft, 2004; Yao & Klug, 2010; Strobel *et al.*, 2009).

Based on this idea, extensive studies have been carried out to explore the likely superconductivity of hydrogen-dominated solids (Tse *et al.*, 2007; Gao, Oganov *et al.*, 2008; Gao *et al.*, 2010; Chen, Struzhkin *et al.*, 2008; Chen, Wang *et al.*, 2008; Yao *et al.*, 2007; Jin *et al.*, 2010; Kim *et al.*, 2008, 2009; Goncharenko *et al.*, 2008; Eremets *et al.*, 2008; Martinez-Canales *et al.*, 2006, 2009; Feng *et al.*, 2006; Degtyareva *et al.*, 2007; Pickard & Needs, 2006). It has been confirmed experimentally (Chen *et al.*, 2008; Eremets *et al.*, 2008) that silane (SiH_4) becomes metallic at around 50–60 GPa, but with a rather low superconducting temperature (Eremets *et al.*, 2008) T_c of 17 K at 96 and 120 GPa, though debate remains (Degtyareva *et al.*, 2009). Theoretical investigations revealed new high-pressure superconducting phases in germane (GH_4) (Gao, Oganov *et al.*, 2008) and stannane (SnH_4) (Gao *et al.*, 2010), with $T_c = 64$ K at 220 GPa for GH_4 and 62 K at 200 GPa for SnH_4. Superconductivity was also reported in disilane (Si_2H_6) (Jin *et al.*, 2010), where T_c reaches 139 K at 300 GPa. Besides the group 14 hydrides, the transition metal hydride YH_3 was predicted to be a superconductor with $T_c = 40$ K at a pressure as low as 17.7 GPa (Kim *et al.*, 2009). Moreover, superconductivity was also reported in AlH_3 (Goncharenko *et al.*, 2008; Rousseau & Bergara, 2010) and PtH (Kim *et al.*, 2011; Scheler *et al.*, 2011; Zhou *et al.*, 2011).

This approach has been extended further by mixing hydrogen molecules with other simple molecules or elements under pressure (Strobel *et al.*, 2009; Wang *et al.*, 2009; Somayazulu *et al.*, 1996). Strobel *et al.* (2009) showed that silane can interact with extra hydrogen molecules to form the high-pressure van der Waals compound $SiH_4(H_2)_2$ at 7 GPa. Remarkably, the H_2 vibrons in $SiH_4(H_2)_2$ soften upon formation of the compound with increasing pressure. This observation indicates that, unlike the repulsive intermolecular interactions in other simple-molecule materials, the covalent band of H_2 is weakened by the unusually strong intermolecular interaction between SiH_4 and H_2, which is attractive in nature and may introduce a metallic phase with properties similar to metallic hydrogen. Indeed, although experiments have not yet observed its metallization, theoretical studies (Li *et al.*, 2010) have predicted that $SiH_4(H_2)_2$ will metallize above 120 GPa with $T_c \simeq 100$ K at 250 GPa. These results encouraged and motivated us to study the wide range of hydrogen-rich materials in order to search for possible high-transition-temperature superconductors.

It is known that, under ambient conditions, LiH is the only hydride between Li and H. However, by applying the *ab initio* evolutionary algorithm USPEX (Oganov & Glass, 2006; Oganov *et al.*, 2006; Glass *et al.*, 2006), a recent study found that Li can absorb more hydrogen under pressure and form a new series of lithium hydrides LiH_n (n = 2, 6, 8) (Zurek *et al.*, 2009). All of them are metals at high pressure and their superconductivity is still unknown. Here, we present a

‡ Current address: Center for Nanophase Materials Science, Oak Ridge National Laboratory, Tennessee, USA.

  doi:10.1107/S2053229613028337

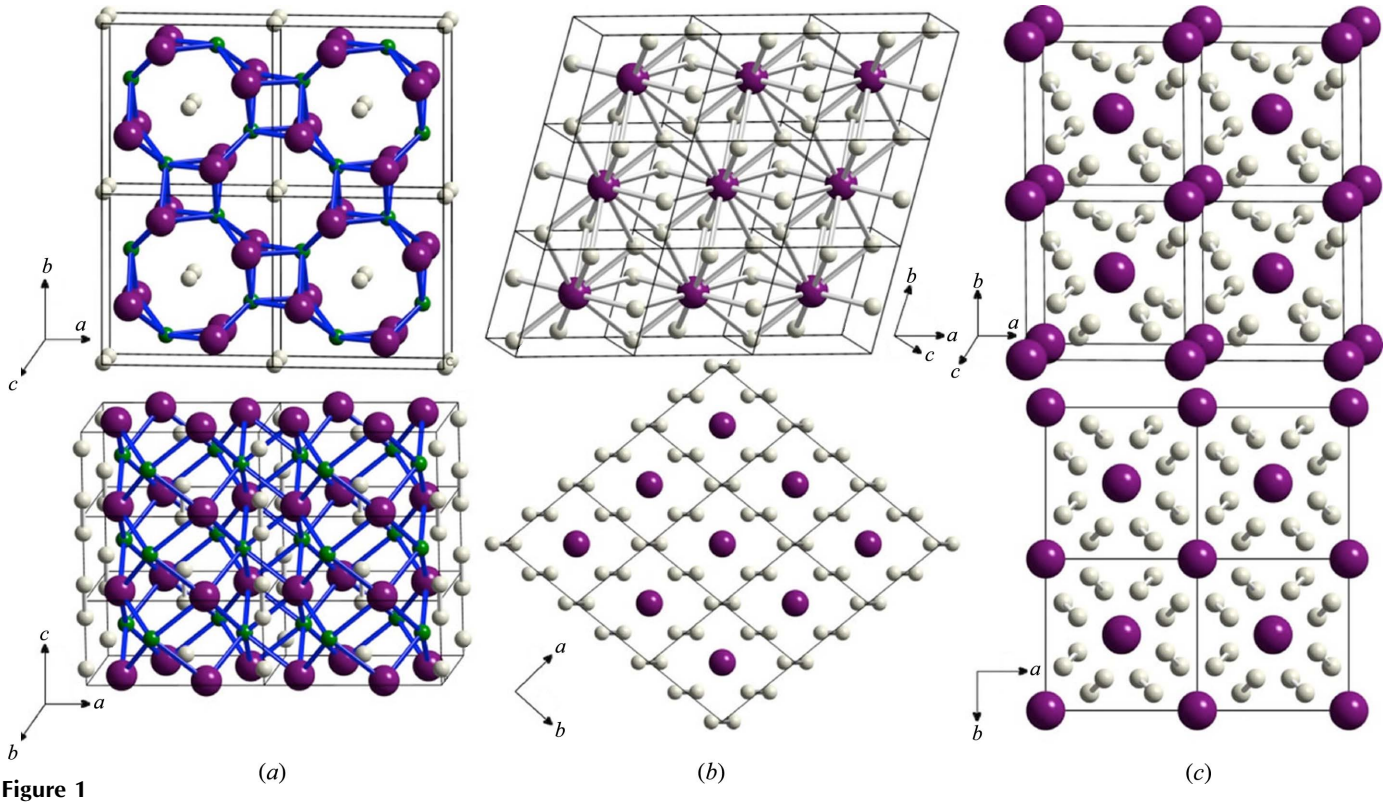

Figure 1
Illustrations of the crystal structures of (*a*) LiH_2, (*b*) LiH_6 and (*c*) LiH_8. Large purple atoms represent Li, hydridic H atoms are shown in green and white represents H atoms belonging to the H_2 units. The blue bonds in LiH_2 show the 'LiH' cage and it is obvious that the H_2 units form a linear chain passing through the centre of the cage. It is also clear that Li is embedded in the H_2 sublattices in LiH_6 and LiH_8.

systematic theoretical investigation of the electronic structures, lattice dynamics and superconductivities of LiH_n at high pressure. We show that the new lithium hydrides are clearly metals under compression, but have different metallization mechanisms. Superconductivity was identified in LiH_6 and LiH_8, with $T_c = 38$ K at 150 GPa for LiH_6 and 31 K at 100 GPa for LiH_8, while LiH_2 is not a superconductor. Electron–phonon coupling (EPC) calculations suggest that the intermolecular vibrations of the H_2 units contribute most to the superconductivity of LiH_6 and LiH_8. Moreover, the T_c of LiH_6 increases with pressure and reaches 82 K at 300 GPa, due to the enhanced electronic density of states (DOS) at the Fermi level (E_F).

2. Computational details

We performed pseudopotential plane-wave calculations based on density functional theory (DFT) (Hohenberg & Kohn, 1964; Kohn & Sham, 1965), as implemented in the *Quantum-ESPRESSO* package (Giannozzi *et al.*, 2009; Scandolo *et al.*, 2005), with the generalized gradient approximation (GGA) of Perdew, Burke and Ernzerhof (PBE) (Perdew *et al.*, 1996; Perdew & Burke, 1986). The Troullier–Martins (Troullier & Martins, 1991) norm-conserving scheme was used to generate the pseudopotentials for H and Li, with the $1s^1$ and $1s^22s^1$ electrons treated as valence electrons, respectively. A plane-wave basis set with an energy cut-off of 80 Ry was used and gave well converged total energies within 5×10^{-5} Ry atom^{-1}. Monkhorst–Pack (MP) (Monkhorst & Pack, 1976) grids of $12 \times 12 \times 24$, $16 \times 16 \times 16$ and $16 \times 16 \times 16$ were adopted for the electronic Brillouin zone (BZ) integration for LiH_2, LiH_6, and LiH_8, respectively. The total number of energy bands for the GW_0 calculation (Shishkin & Kresse, 2006) is 240.

Lattice dynamics and electron–phonon coupling were computed using the density functional perturbation theory (DFPT) (Giannozzi *et al.*, 2009; Baroni *et al.*, 2001). Subsequently, in order to interpolate the interatomic force constant (IFC) matrix for the phonon dispersions, $4 \times 4 \times 8$, $8 \times 8 \times 8$ and $8 \times 8 \times 8$ q-meshes in the first BZ were used for interpolation for LiH_2, LiH_6 and LiH_8, respectively. The denser $24 \times 24 \times 48$, $32 \times 32 \times 32$ and $32 \times 32 \times 32$ grids were sufficient to ensure the convergence of the double-δ function needed for the EPC calculations for the three lithium hydrides, respectively. Note that the same EPC technique was applied earlier to other systems and reliable estimates of the superconducting transition temperature T_c were achieved (Gao, Xie *et al.*, 2008; Ma *et al.*, 2004; Wang, Lv *et al.*, 2009; Xu *et al.*, 2007). The lattice parameters and atomic coordinates were fully optimized before these calculations.

3. Results and discussion

The calculated structures of the lithium hydrides LiH_2, LiH_6 and LiH_8 are illustrated in Fig. 1, and the corresponding lattice parameters are listed in Table 1. LiH_2 becomes stable above 130 GPa and adopts a structure in the space group $P4/mbm$,

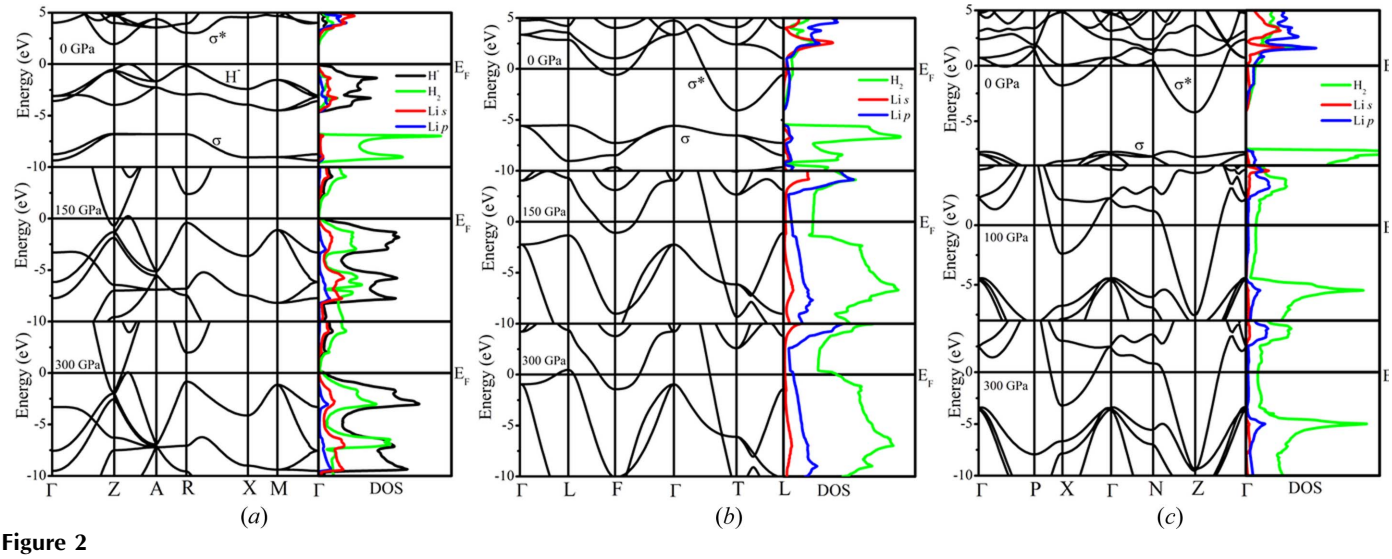

Figure 2
The evolution with pressure of the band structure and projected electronic DOS of (*a*) LiH_2, (*b*) LiH_6 and (*c*) LiH_8, shown at selected pressures. H^-, σ and σ^* indicate the contributor to the different electronic bands.

with four formula units (f.u.) per unit cell (Li_4H_8) (Zurek *et al.*, 2009). As can be seen in Fig. 1(*a*), there are two types of hydrogen site: H1 (green) and H2 (white) occupy 4*f* and 4*e* sites, respectively. Li forms bonds with the nearest H1 atom, while H2 atoms form H_2 units. The H—H bond length in the H_2 units is 0.76 Å at 150 GPa, which is slightly longer than that in pure solid H_2 (0.737 Å; Pickard & Needs, 2007). Moreover, the H—H distance is compressed by only 0.02 Å at 300 GPa, indicating that the interaction between the H_2 units and the 'LiH' framework may be weak. Furthermore, LiH_2 can be considered as a host–guest structure (McMahon & Nelmes, 2006), where Li and H1 atoms form the 'cage' and H2 atoms are trapped inside: $4LiH + 2H_2$. LiH_6 and LiH_8 are predicted to be stable at pressures above 140 GPa and between 100 and 200 GPa, and exhibit structures in the space groups $R\bar{3}m$ and $I\bar{4}22$, respectively (Zurek *et al.*, 2009). Remarkably, both LiH_6 and LiH_8 have just one f.u. in the primitive cell, so that there are odd numbers of electrons in the cell. In contrast with LiH_2, all the H atoms in LiH_6 and LiH_8 form H_2 units and Li can be viewed as intercalated in the H_2 sublattice. At zero pressure, the shortest H—H distances are 0.81 and 0.79 Å for LiH_6 and LiH_8, respectively. Compared with pure H_2, the bond lengths of the H_2 units in LiH_6 and LiH_8 are significantly stretched. This may be induced by the strong interaction between Li and H_2 units, which has been seen in $SiH_4(H_2)_2$ (Strobel *et al.*, 2009). On compression, the H—H distances are elongated by 0.02 and 0.015 Å for LiH_6 and LiH_8 at 300 and 200 GPa, respectively.

All three of these lithium hydrides are metals at high pressure, with different metallization mechanisms (Zurek *et al.*, 2009), as shown in Fig. 2. For LiH_2, the pressure-induced band overlap is responsible for metallization (Fig. 2*a*). The PBE band gap is closed around 50 GPa, which is much lower than the theoretical metallization pressure of ∼240 GPa for pure hydrogen gas (Pickard & Needs, 2007). However, it is well known that DFT usually underestimates the band gap of a material. Therefore, we studied the band gap of LiH_2 as a function of pressure using the GW_0 approximation. From Fig. 3, it is obvious that the PBE band gap is smaller than the

Table 1
Lattice parameters and atomic coordinates for LiH_2, LiH_6 and LiH_8 at 150, 150 and 100 GPa, respectively.

H1 and H2 represent the hydridic hydrogen and H_2 units in LiH_2, respectively.

Compound and space group	Pressure (GPa)	Lattice parameters (Å, °)	Atomic coordinates (fractional)
LiH_2, *P*4/*mbm*	150	*a* = 4.084	Li 4*g* (0.3446 0.8446 0.0000)
		c = 1.957	H1 4*f* (0.1480 0.6480 0.5000)
			H2 4*e* (0.0000 0.0000 0.8054)
LiH_6, $R\bar{3}m$	150	*a* = 2.565	Li 3*b* (0.0000 0.0000 0.5000)
		α = 75.204	H 18*h* (0.6681 0.8343 0.7582)
LiH_8, $I\bar{4}22$	100	*a* = 3.433	Li 2*a* (0.0000 0.0000 0.0000)
		b = 3.821	H 16*k* (0.3850 0.2112 0.8501)

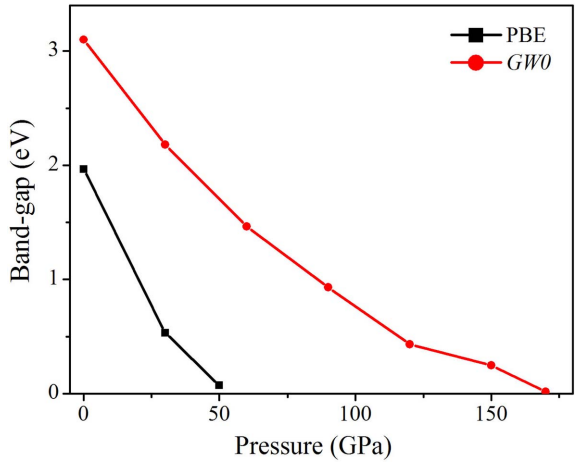

Figure 3
Evolution of the PBE and GW_0 band gaps of LiH_2 as a function of pressure. Clearly, GW_0 predicts a much higher metallization pressure than PBE.

GW_0 band gap, and the latter remains open up to 170 GPa. Although the GW_0 metallization pressure of LiH_2 is higher than that of PBE, it is still lower than that for pure hydrogen gas, predicted to be between 240 and 260 GPa (Lebègue *et al.*, 2012). In contrast with LiH_2, one can observe that LiH_6 and LiH_8 are native metals (Figs. 2*b* and 2*c*), and the H_2 σ* states cross the Fermi level (E_F), even at pressures where they are thermodynamically unstable against decomposition into LiH and H_2. The partially filled H_2 σ* state corresponds to electron transfer from Li due to the strong intermolecular interaction between Li and the H_2 unit (Zurek *et al.*, 2009). This metallization mechanism is quite different from other hydrogen-rich materials, where it is a result of band overlap on compression, and it may provide a new pathway to metallize hydrogen. At higher pressure, charge transfer still dominates and the σ and σ* bands overlap just like in LiH_2. It is worth noting that the σ band crosses E_F in LiH_6 along the Γ–L direction under further compression, due to hybridization of the σ and σ* orbitals. This is not observed in the pressure range of stability of LiH_8 due to the deeper H_2 σ bands.

Phonon calculations did not give any imaginary frequencies, indicating dynamic stability of all three lithium hydrides (Fig. 4). From the phonon band structure and site-projected phonon DOS (Fig. 4), it is found that the low-energy phonon modes are mainly associated with Li atoms due to their greater atomic mass. The intermediate frequencies correspond to intermolecular vibrations, while above 2500 cm^{-1} the H_2 intramolecular vibrations dominate. The highest phonon frequencies are 3990, 3164 and 3341 cm^{-1} for LiH_2, LiH_6 and LiH_8 at 150, 150 and 100 GPa, respectively. Compared with

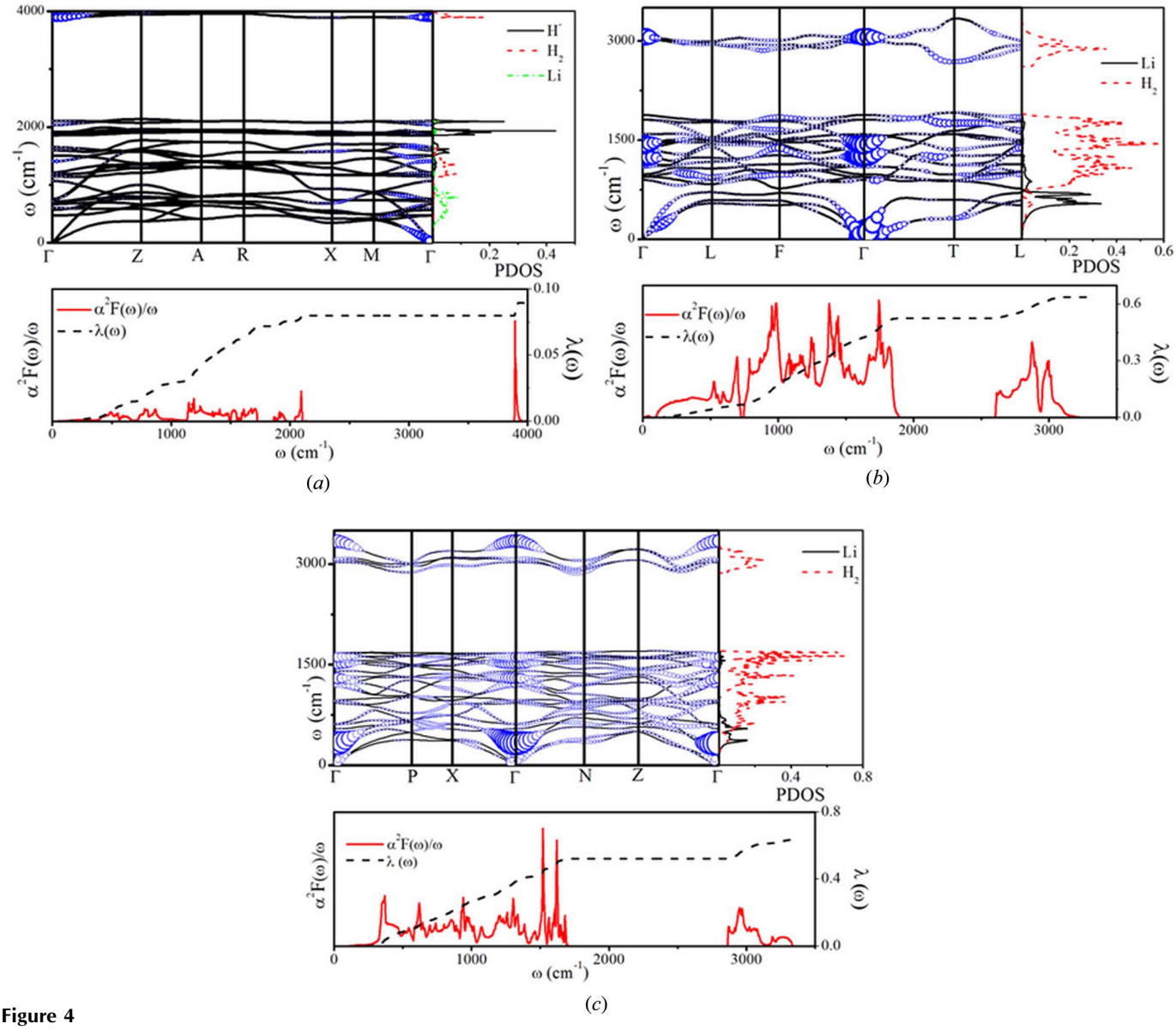

Figure 4
The upper panels of (*a*), (*b*) and (*c*) are the calculated phonon dispersion and site-projected phonon DOS of LiH_2, LiH_6 and LiH_8 at 150, 150 and 100 GPa, respectively. The area of each circle is proportional to the partial EPC parameter $\lambda(\omega_{qj})$. Clearly, all the phonon modes contribute to the EPC parameter, indicating an isotropic system. The phonon spectroscopic function $\alpha^2F(\omega)/\omega$ and the EPC parameter integral are presented in the lower panels. It is obvious that the intermolecular vibrations of the H_2 units are the main contributor to the EPC parameter λ.

the free H_2 vibron of 4161 cm^{-1} (Stoicheff, 1957), the H_2 vibron is hardly changed in LiH_2 since the H—H distance is only slightly stretched, and it is reduced in LiH_6 and LiH_8 due to the longer H—H bond, similar to what was seen in $SiH_4(H_2)_2$ (Strobel *et al.*, 2009). Upon further compression, all the phonon frequencies harden due to increasing intermolecular interaction.

The superconductivity of the three lithium hydrides can be conveniently studied by EPC calculation. The key issue in the calculation of the EPC parameter λ is the Eliashberg phonon spectroscopic function $\alpha^2F(\omega)$, which can be expressed in terms of the phonon line width γ_{qj} owing to electron–phonon scattering (Allen, 1972; Allen & Silberglitt, 1974)

$$\alpha^2F(\omega) = \frac{1}{2\pi N_f}\sum_{qj}\frac{\gamma_{qj}}{\omega_{qj}}\delta(\hbar\omega - \hbar\omega_{qj}), \quad (1)$$

where N_f is the electronic DOS per atom at the E_F, q is a wavevector in the first BZ, j is the phonon mode label and ω_{qj} is the phonon frequency of mode qj. The EPC parameter λ can be defined as the first reciprocal moment of the spectroscopic function $\alpha^2F(\omega)$

$$\lambda = 2\int_0^\infty \frac{\alpha^2F(\omega)}{\omega}\,d\omega = 2\int_0^\infty d\omega\lambda(\omega_{qj}) = \sum_{qj}\lambda(\omega_{qj}), \quad (2)$$

$$\lambda(\omega_{qj}) = \frac{\alpha^2F(\omega_{qj})}{\omega_{qj}} = \frac{\gamma_{qj}}{\pi N_f\omega_{qj}^2}, \quad (3)$$

where $\lambda(\omega_{qj})$ is the partial EPC parameter of phonon mode q_j.

The calculated spectroscopic function $\alpha^2F(\omega)/\omega$ and integration of the EPC parameter λ are shown in Fig. 4 for LiH_2, LiH_6 and LiH_8 at 150, 150 and 100 GPa, respectively. One can see from the partial EPC parameter $\lambda(\omega_{qj})$ that all phonon modes have contributed to the overall EPC parameter λ, showing a three-dimensional nature to the structure. Therefore, the conventional one-band theory is sufficient to determine the critical transition temperature (Pickett, 2002).

Table 2
The calculated logarithmic average phonon frequency (ω_{log}), EPC parameter (λ) and critical temperature T_c (μ^* = 0.13) for LiH_2, LiH_6 and LiH_8 at 150, 150 and 100 GPa, respectively.

	Pressure (GPa)	λ	ω_{log} (K)	T_c (K)
LiH_2	150	0.0890	1740.8	0.00
LiH_6	150	0.6387	1911.9	38.34
LiH_8	100	0.6353	1576.8	31.04

The superconducting T_c can be estimated from the Allen–Dynes modified McMillan equation (McMillan, 1968; Allen & Dynes, 1975)

$$T_c = \frac{\omega_{log}}{1.2}\exp\left[-\frac{1.04(1+\lambda)}{\lambda - \mu^*(1+0.62\lambda)}\right], \quad (4)$$

where ω_{log} is the logarithmic average phonon frequency,

$$\omega_{log} = \exp\frac{2}{\lambda}\int_0^\omega \frac{\alpha^2F(\omega)\ln\omega}{\omega}\,d\omega, \quad (5)$$

and a typical value of the Coulomb pseudopotential μ^* = 0.13 is used. The calculated T_c, λ and ω_{log} at selected pressures for the three lithium hydrides are listed in Table 2. Not surprisingly, LiH_2 is not a superconductor due to the small λ. This is because the DOS near E_F is very small, so that there are not enough electrons to form Cooper pairs (Cooper, 1956) connected by the phonons. LiH_6 and LiH_8 are superconductors with relatively high T_c values of 38 and 31 K at 150 and 100 GPa, respectively. Looking at the spectroscopic function $\alpha^2F(\omega)/\omega$, it is obvious that the main contributors are the intermediate intermolecular vibrations between H_2 units. Nearly 75% of λ originates from this region. With increasing pressure, it is very interesting to note that, despite a decrease in ω_{log}, λ increases dramatically above 250 GPa, resulting in an enhanced T_c for LiH_6, as shown in Fig. 5(*a*). The T_c value for LiH_6 reaches as high as 82 K at 300 GPa, twice as high as the T_c value at 150 GPa, and this is comparable with molecular metallic hydrogen with $T_c \simeq 100$ K (Zhang *et al.*, 2007; Cudazzo *et al.*, 2008) above 350 GPa. From Fig. 5(*b*), one can

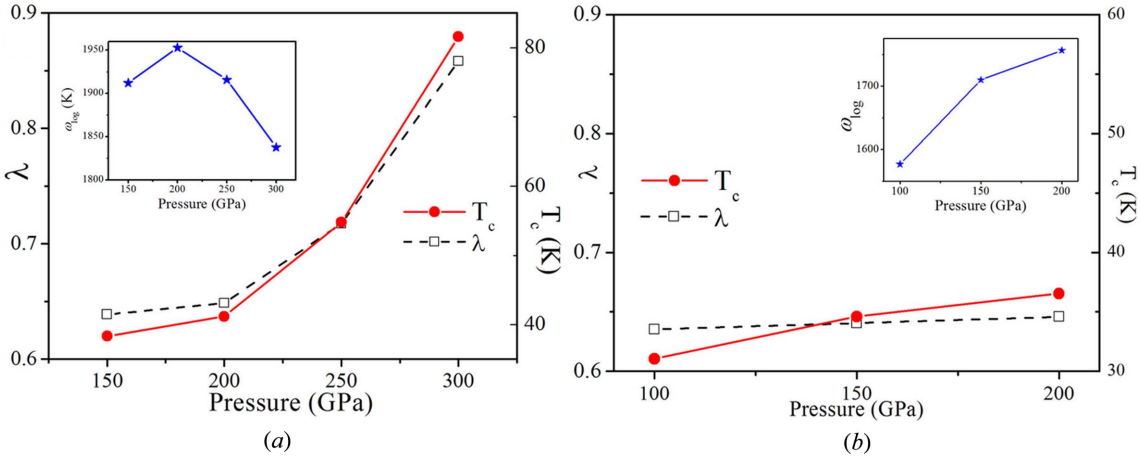

Figure 5
Pressure dependence of the transition temperature T_c, EPC parameter λ and logarithmic average phonon frequency ω_{log} for (*a*) LiH_6 and (*b*) LiH_8. Dramatic increases in λ and T_c with pressure are observed for LiH_6.

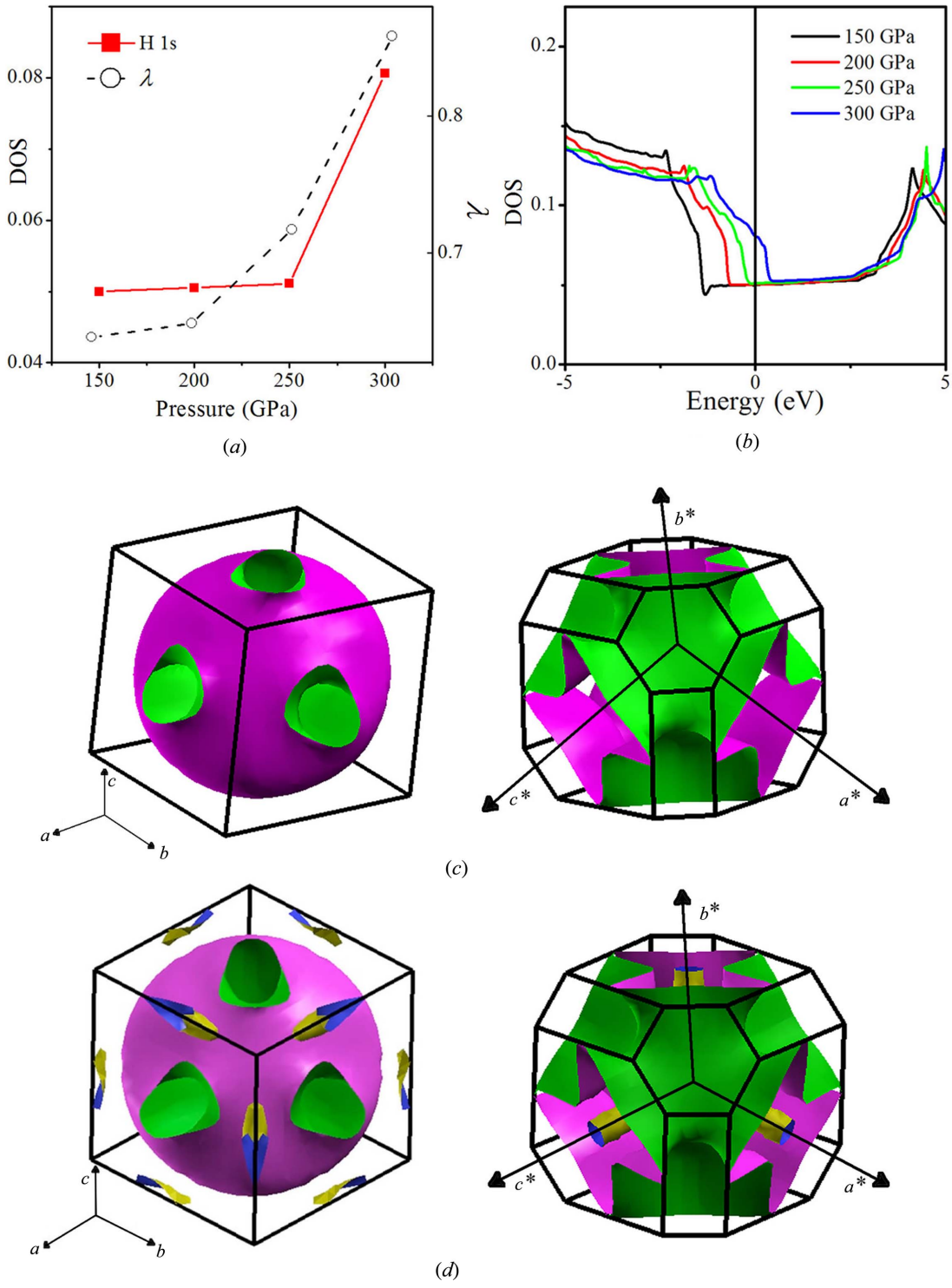

Figure 6
(*a*)/(*b*) The evolution of the electronic DOS at E_F and in the vicinity of E_F compared with the EPC parameter λ of LiH_6. λ is enhanced by the continuous increase in the σ character of the DOS near E_F, corresponding to band hybridization. The topology of the FS is shown in the reciprocal cell (left panel) and in the first BZ (right panel) at (*c*) 150 and (*d*) 300 GPa. An additional FS appears at 300 GPa due to a σ band crossing E_F at high pressure.

observe that the T_c of LiH_8 increases slightly due to the increase in ω_{log} corresponding to the enhanced phonon frequencies.

Why has λ changed so much in LiH_6 under compression? As we know, the EPC parameter λ describes the electron–phonon coupling strength (Bardeen *et al.*, 1957) which is associated with electrons in the vicinity of E_F. Therefore, the pressure evolution of the DOS near E_F and the topology of the Fermi surface (FS) have been studied to probe the origin of enhanced λ. At 150 GPa, E_F is located at the bottom of a

pseudogap of the electronic DOS. Only the σ^* band crosses E_F and forms a free-electron-like three-dimensional FS, with open holes open in the T–L direction showing an electron-like character (Fig. 6*c*). As the pressure is increased, the σ bands move towards E_F, as observed previously. More and more electrons entering the vicinity of E_F induce a continual increase in λ. Above 250 GPa, an extra flat σ band crosses E_F along the Γ–L direction, introducing an additional 'pocket-like' FS with a hole-type character (Fig. 6*d*). The simultaneous occurrence of a flat band near E_F has been generally observed in high-temperature cuprate superconductors (Simon, 1997). This feature has been suggested as a favourable condition for enhancing electron–hole pairing, which is essential to superconductivity (Zhang *et al.*, 2010). Therefore, the increase in λ originates from the increased DOS near E_F, corresponding to the hybridization of the H_2 σ and σ^* orbitals. It can be expected that λ will be further enhanced, since more σ bands will cross E_F and an even higher T_c can be expected at higher pressure.

4. Conclusion

In summary, we have extensively examined the lattice dynamics and superconductivity of newly proposed lithium hydrides by means of *ab initio* calculations. LiH_2 is predicted to become a metal above 170 GPa by *GW* calculations, which is much higher than the PBE method predicts. The predicted metallization pressures of LiH_2, LiH_6 and LiH_8 are lower than for pure hydrogen gas. In particular, the latter two are native metals. The high-pressure stability of these three lithium hydrides is confirmed by their non-imaginary phonon frequencies. Based on conventional BCS theory, LiH_2 is predicted to be a nonsuperconductor, whereas the other two hydrides are superconductors. The calculated T_c values are 38 and 31 K for LiH_6 and LiH_8 at 150 and 100 GPa, respectively. With increasing pressure, the T_c value for LiH_6 is enhanced and reaches 82 K at 300 GPa, corresponding to increased H_2 σ character near E_F. No major changes are observed in LiH_8. Our results may provide some insight for the metallization of pure hydrogen, and future experiments to explore the metallicity and superconductivity of high-pressure lithium hydrides are highly desirable.

The authors are grateful for support of this work from the National Natural Science Foundation of China (grant Nos. 10874054, 91022029 and 11025418), the National High-Tech ICF Committee in China, and the Research Fund from the Laboratory of Science and Technology on Surface Physics and Chemistry (grant No. SPC201103).

References

Allen, P. B. (1972). *Phys. Rev. B*, **6**, 2577–2579.
Allen, P. B. & Dynes, R. C. (1975). *Phys. Rev. B*, **12**, 905–922.
Allen, P. B. & Silberglitt, R. (1974). *Phys. Rev. B*, **9**, 4733–4741.
Ashcroft, N. W. (1968). *Phys. Rev. Lett.* **21**, 1748–1749.
Ashcroft, N. W. (2004). *Phys. Rev. Lett.* **92**, 187002.
Barbee, T. W. III, Cohen, M. L. & Martins, J. L. (1989). *Phys. Rev. Lett.* **62**, 1150–1153.
Bardeen, J., Cooper, L. N. & Schrieffer, J. R. (1957). *Phys. Rev.* **108**, 1175–1204.
Baroni, S., de Gironcoli, S., Dal Corso, A. & Giannozzi, P. (2001). *Rev. Mod. Phys.* **73**, 515–562.
Chen, X. J., Struzhkin, V. V., Song, Y., Goncharov, A. F., Ahart, M., Liu, Z., Mao, H. K. & Hemley, R. J. (2008). *Proc. Natl Acad. Sci. USA*, **105**, 20–23.
Chen, X. J., Wang, J. L., Struzhkin, V. V., Mao, H. K., Hemley, R. J. & Lin, H. Q. (2008). *Phys. Rev. Lett.* **101**, 077002.
Cooper, L. N. (1956). *Phys. Rev.* **104**, 1189–1190.
Cudazzo, P., Profeta, G., Sanna, A., Floris, A., Continenza, A., Massidda, S. & Gross, E. K. U. (2008). *Phys. Rev. Lett.* **100**, 257001.
Degtyareva, O., Martínez-Canales, M., Bergara, A., Chen, X.-J., Song, Y., Struzhkin, V. V., Mao, H.-K. & Hemley, R. J. (2007). *Phys. Rev. B*, **76**, 064123.
Degtyareva, O., Proctor, J. E., Guillaume, C. L., Gregoryanz, E. & Hanfland, M. (2009). *Solid State Commun.* **149**, 1583–1586.
Eremets, M. I., Trojan, I. A., Medvedev, S. A., Tse, J. S. & Yao, Y. (2008). *Science*, **319**, 1506–1509.
Feng, J., Grochala, W., Jaroń, T., Hoffmann, R., Bergara, A. & Ashcroft, N. W. (2006). *Phys. Rev. Lett.* **96**, 017006.
Gao, G., Oganov, A. R., Bergara, A., Martinez-Canales, M., Cui, T., Iitaka, T., Ma, Y. & Zou, G. (2008). *Phys. Rev. Lett.* **101**, 107002.
Gao, G., Oganov, A. R., Li, P., Li, Z., Wang, H., Cui, T., Ma, Y., Bergara, A., Lyakhov, A. O., Iitaka, T. & Zou, G. (2010). *Proc. Natl Acad. Sci. USA*, **107**, 1317–1320.
Gao, G., Xie, Y., Cui, T., Ma, Y., Zhang, L. & Zou, G. (2008). *Solid State Commun.* **146**, 181–185.
Giannozzi, P. *et al.* (2009). *J. Phys. Condens. Matter*, **21**, 395502.
Glass, C. W., Oganov, A. R. & Hansen, N. (2006). *Comput. Phys. Commun.* **175**, 713–720.
Goncharenko, I., Eremets, M. I., Hanfland, M., Tse, J. S., Amboage, M., Yao, Y. & Trojan, I. A. (2008). *Phys. Rev. Lett.* **100**, 045504.
Goncharov, A. F., Gregoryanz, E., Hemley, R. J. & Mao, H. (2001). *Proc. Natl Acad. Sci. USA*, **98**, 14234–14237.
Hohenberg, P. & Kohn, W. (1964). *Phys. Rev.* **136**, B864–B871.
Jin, X., Meng, X., He, Z., Ma, Y., Liu, B., Cui, T. Z., Zou, G. & Mao, H. K. (2010). *Proc. Natl Acad. Sci. USA*, **107**, 9969–9973.
Kim, D. Y., Scheicher, R. H. & Ahuja, R. (2009). *Phys. Rev. Lett.* **103**, 077002.
Kim, D. Y., Scheicher, R. H., Lebègue, S., Prasongkit, J., Arnaud, B., Alouani, M. & Ahuja, R. (2008). *Proc. Natl Acad. Sci. USA*, **105**, 16454–16459.
Kim, D. Y., Scheicher, R. H., Pickard, C. J., Needs, R. J. & Ahuja, R. (2011). *Phys. Rev. Lett.* **107**, 117002.
Kohn, W. & Sham, L. J. (1965). *Phys. Rev.* **140**, A1133–A1138.
Lebègue, S., Araujo, C. M., Kim, D. Y., Ramzan, M., Mao, H. K. & Ahuja, R. (2012). *Proc. Natl Acad. Sci. USA*, **109**, 9766–9769.
Li, Y., Gao, G., Xie, Y., Ma, Y., Cui, T. & Zou, G. (2010). *Proc. Natl Acad. Sci.* **107**, 15708–15711.
Loubeyre, P., Occelli, F. & LeToullec, R. (2002). *Nature*, **416**, 613–617.
Ma, Y., Tse, J. S., Klug, D. D. & Ahuja, R. (2004). *Phys. Rev. B*, **70**, 214107.
Martinez-Canales, M., Bergara, A., Feng, J. & Grochala, W. (2006). *J. Phys. Chem. Solids*, **67**, 2095–2099.
Martinez-Canales, M., Oganov, A. R., Ma, Y., Yan, Y., Lyakhov, A. O. & Bergara, A. (2009). *Phys. Rev. Lett.* **102**, 87005.
McMahon, M. I. & Nelmes, R. J. (2006). *Chem. Soc. Rev.* **35**, 943–963.
McMillan, W. (1968). *Phys. Rev.* **167**, 331–344.
Monkhorst, H. J. & Pack, J. D. (1976). *Phys. Rev. B*, **13**, 5188–5192.
Oganov, A. R. & Glass, C. W. (2006). *J. Chem. Phys.* **124**, 244704.
Oganov, A. R., Glass, C. W. & Ono, S. (2006). *Earth Planet. Sci. Lett.* **241**, 95–103.
Perdew, J. P. & Burke, K. (1996). *Int. J. Quantum Chem.* **57**, 309–319.
Perdew, J. P., Burke, K. & Ernzerhof, M. (1996). *Phys. Rev. Lett.* **77**, 3865–3868.
Pickard, C. J. & Needs, R. J. (2006). *Phys. Rev. Lett.* **97**, 045504.
Pickard, C. J. & Needs, R. J. (2007). *Nature Phys.* **3**, 473–476.
Pickett, W. (2002). *Nature*, **418**, 733–734.
Rousseau, B. & Bergara, A. (2010). *Phys. Rev. B*, **82**, 104504.
Scandolo, S., Giannozzi, P., Cavazzoni, C., de Gironcoli, S., Pasquarello, A. & Baroni, S. (2005). *Z. Kristallogr.* **220**, 574–579.
Scheler, T., Degtyareva, O., Marqués, M., Guillaume, C. L., Proctor, J. E., Evans, S. & Gregoryanz, E. (2011). *Phys. Rev. B*, **83**, 214106.
Shishkin, M. & Kresse, G. (2006). *Phys. Rev. B*, **74**, 035101.
Simon, A. (1997). *Angew. Chem. Int. Ed. Engl.* **36**, 1788–1806.
Somayazulu, M. S., Finger, L. W., Hemley, R. J. & Mao, H. K. (1996). *Science*, **271**, 1400–1402.
Stoicheff, B. P. (1957). *Can. J. Phys.* **35**, 730–741.
Strobel, T. A., Somayazulu, M. & Hemley, R. J. (2009). *Phys. Rev. Lett.* **103**, 065701.

Troullier, N. & Martins, J. L. (1991). *Phys. Rev. B*, **43**, 1993–2006.
Tse, J. S., Yao, Y. & Tanaka, K. (2007). *Phys. Rev. Lett.* **98**, 117004.
Wang, Y., Lv, J., Ma, Y., Cui, T. & Zou, G. (2009). *Phys. Rev. B*, **80**, 092505.
Wang, S., Mao, H. K., Chen, X. J. & Mao, W. L. (2009). *Proc. Natl Acad. Sci. USA*, **106**, 14763–14767.
Wigner, E. & Huntington, H. B. (1935). *J. Chem. Phys.* **3**, 764–770.
Xu, Y., Zhang, L., Cui, T., Li, Y., Xie, Y., Yu, W., Ma, Y. & Zou, G. (2007). *Phys. Rev. B*, **76**, 214103.
Yao, Y. & Klug, D. D. (2010). *Proc. Natl Acad. Sci. USA*, **107**, 20893–20898.
Yao, Y., Tse, J. S., Ma, Y. & Tanaka, K. (2007). *Europhys. Lett.* **78**, 37003.
Zhang, C., Chen, X. J., Li, Y. L., Struzhkin, V. V., Mao, H. K., Zhang, R. Q. & Lin, H. Q. (2010). *Europhys. Lett.* **90**, 66006.
Zhang, L., Niu, Y., Li, Q., Cui, T., Wang, Y., Ma, Y., He, Z. & Zou, G. (2007). *Solid State Commun.* **141**, 610–614.
Zhou, X.-F., Oganov, A. R., Dong, X., Zhang, L., Tian, Y. & Wang, H.-T. (2011). *Phys. Rev. B*, **84**, 054543.
Zurek, E., Hoffmann, R., Ashcroft, N. W., Oganov, A. R. & Lyakhov, A. O. (2009). *Proc. Natl Acad. Sci. USA*, **106**, 17640–17643.

supplementary materials